A Zonally Averaged Ocean Model for the Thermohaline Circulation. Part I: Model Development and Flow Dynamics

DANIEL G. WRIGHT* AND THOMAS F. STOCKER

Centre for Climate and Global Change Research, Department of Meteorology, McGill University, Montreal, Quebec, Canada

(Manuscript received 4 September 1990, in final form 10 April 1991)

ABSTRACT

A two-dimensional latitude–depth ocean model is developed on the basis of the zonally averaged balance equations of mass, momentum, heat, and salt. Its purpose is to investigate the dynamics and variability of the buoyancy-forced thermohaline circulation. For the time scales of interest an annually averaged model is selected, and the momentum balance is taken to be diagnostic. The east–west pressure gradient, which arises upon zonally averaging the momentum equations, is parameterized in terms of the meridional pressure gradient.

The thermohaline circulation is driven by mixed surface boundary conditions, i.e., temperatures are relaxed to prescribed values while the salt flux is held constant. The dynamics of the flow is investigated in hemispheric and global geometries for both short and long time integrations, the latter extending over many thousands of years.

As has been noted by previous investigators, it is possible to perturb a steady state such that a diffusively dominated regime results. By considering a simple analytic model for the diffusive state in an ocean with a linear equation of state, it is demonstrated that any steady, diffusive state is unstable. Convective overturning must occur either at low or at high latitudes. In the former case adjustments are minor, whereas high latitude convection can result in a basinwide rearrangement of the water masses. These two different processes are verified in the present model; violent overturning repeats about every 20 000 years. The application of the model as a component of a two-dimensional paleoclimate model is discussed.

1. Introduction

Until recently, the World Ocean was commonly considered to play only a passive role as a component of the climate system, simply acting as a reservoir of heat and water. During the last few years, however, new attention has been focused on the variability of the ocean circulation in relation to climatic change. In particular, the thermohaline circulation has been recognized as a key part in the interactions of the atmosphere, cryosphere, and hydrosphere (Broecker and Denton 1989). The implementation of more sophisticated oceanic components into climate models is therefore necessary. In presenting a zonally averaged ocean model, we hope that the present paper is a contribution toward this task.

Studies of the atmospheric circulation and energy balance imply that about 50% [i.e., 2 to 3 PW (1 PW = 10^{15} W)] of the global meridional heat transport is carried through the World Ocean. Unlike in the atmosphere, the heat flux in the ocean is mainly due to the mean meridional overturning, as confirmed by various general circulation models (e.g., Bryan 1987; Manabe and Stouffer 1988) and observational studies (Hall and Bryden 1982; Wunsch 1984).

A qualitative understanding of this density-driven circulation was provided by Stommel (1961). He demonstrated, using a box model, that two different states of the oceanic system are possible under identical forcing. They correspond to a direct and an indirect circulation, whereby high-latitude cold water is sinking in the former and low-latitude warm but saline water is sinking in the latter. Associated with these states are meridional heat fluxes in different directions. Whereas the direct cell carries heat poleward, the opposite is true for the indirect cell.

Rooth (1982) extended Stommel's model including two polar boxes and one equatorial box with a deep connection between the polar boxes. A three-box model allowing for deep flow between the polar and equatorial boxes was studied by Welander (1986). Of nine possible solutions for the dynamical system, four are stable. These are the direct and the indirect symmetric modes and two pole-to-pole circulations with deep water forming either in the Northern or the Southern Hemisphere.

The Bryan–Cox Ocean General Circulation Model (OGCM) was used by Bryan (1986) to test the validity of the conclusions based on the earlier conceptual box

* Visiting from: *Department of Fisheries and Oceans, Bedford Institute of Oceanography, Dartmouth, Nova Scotia, Canada.*

Corresponding author address: Dr. Daniel G. Wright, Bedford Institute of Oceanography, Dartmouth, Nova Scotia, Canada, B2Y 4A2.

models. He found three different "steady" states under *mixed boundary conditions,* i.e., surface temperatures are relaxed to specified values, whereas the surface salt flux is fixed. The first state, to which the model converges under *restoring boundary conditions* (both temperature and salinity are relaxed to specified values) shows two hemispheric cells. Deep water is formed at high latitudes in both hemispheres, and upwelling occurs in low latitudes; the meridional heat flux is symmetric. The two other states consist of only one global cell with downwelling in one hemisphere and upwelling in the other. The corresponding meridional heat flux is asymmetric in this case. Manabe and Stouffer (1988) mention that an additional steady state may exist in Bryan's (1986) model. This state has a weak and shallow thermohaline circulation with an intense halocline at high latitudes. Unless salt is added in high latitudes, the symmetric state collapses to this weak circulation (Bryan 1986).

Marotzke et al. (1988, henceforth MWW) developed a two-dimensional, zonally averaged ocean model and showed that the symmetric two-cell circulation is unstable and undergoes a transition to a one-cell circulation when the boundary condition on salinity is switched from restoring to flux type. Thus, both Bryan (1986) and MWW present results that indicate the symmetric two-cell circulation obtained under restoring boundary conditions is unstable upon a switch to mixed boundary conditions. Welander (1986), however, predicts this state to be stable; this is due to the lack of vertical structure in the simple box model. In a later study, Marotzke (1989) showed that the collapse of the thermohaline circulation observed by Bryan could be reproduced by the two-dimensional model of MWW. He then demonstrated the important result that, in both two- and three-dimensional ocean models, this diffusively dominated state is actually very slowly evolving and eventually exhibits a dramatic instability.

Weaver and Sarachik (1991a,b) explore the dynamics of the thermohaline circulation in a 33-level Bryan–Cox OGCM. Long integrations (>7000 surface years, 21 000 bottom years) were performed in both hemispheric and global basins. The model confirms the temporal and spatial variability of the thermohaline circulation; different scenarios are observed, such as successions of violent overturning (*flushes*) occurring on a time scale of 100 to 1000 years; also decadal variability is present. Eventually, a one-cell steady state is realized in both hemispheric and global basin runs.

The purpose of this paper is threefold. First, a zonally averaged, latitude–depth ocean model is developed on the basis of the balance equations of momentum, mass, heat, and salt. The focus of the model is the thermohaline circulation and its variability. Second, we investigate the flow dynamics of the present model under mixed boundary conditions and verify the findings of MWW, Marotzke (1989), and others. Third, we apply the model in Part II (Stocker and Wright 1991) to study the interocean thermohaline circulation in a Pacific–Atlantic basin system.

The paper is organized as follows. Section 2 presents the model development. The numerical procedure is briefly described in section 3. Section 4 deals with the model spinup and some comparisons with previous thermohaline circulation models using mixed boundary conditions. Section 5 examines the diffusively dominated state and its ultimate instability. Conclusions follow in section 6.

2. Formulation of the two-dimensional ocean model

a. Balance equations and boundary conditions

We consider a Boussinesq ocean of uniform depth H and angular width $\Delta\Lambda$. The inertial terms are assumed negligible, and the hydrostatic approximation is made. It is shown below that horizontal viscosity is not needed to satisfy the conditions of no flow through lateral boundaries, so it is neglected. Vertical diffusion of momentum is included, but it plays a minor role. Seasonal and higher frequency variations are not considered, therefore, the momentum equations reduce to diagnostic balances. Temperature and salinity evolution are governed by advection–diffusion equations with constant horizontal and vertical diffusion coefficients, $K_H = 10^3\ \mathrm{m^2\ s^{-1}}$ and $K_V = 0.4 \times 10^{-4}\ \mathrm{m^2\ s^{-1}}$. The density is related to temperature and salinity by a linear equation of state.

To obtain an appropriate set of zonally averaged equations, we write the equations in spherical coordinates and apply the operator

$$(\bar{\ }) = \frac{1}{\lambda_E - \lambda_W} \int_{\lambda_W}^{\lambda_E} d\lambda, \tag{1}$$

where λ_W and λ_E are the longitudes of the western and eastern boundaries. Assuming no material or diffusive flux through λ_W and λ_E, the following set of equations is obtained:

$$-2s\Omega\bar{v} = -\frac{1}{\rho_* ac}\frac{\Delta p}{\Delta\Lambda} + \frac{\partial}{\partial z}\left(\frac{A}{H^2}\frac{\partial \bar{u}}{\partial z}\right), \tag{2}$$

$$2s\Omega\bar{u} = -\frac{c}{\rho_* a}\frac{\partial \bar{p}}{\partial s} + \frac{\partial}{\partial z}\left(\frac{A}{H^2}\frac{\partial \bar{v}}{\partial z}\right), \tag{3}$$

$$\frac{\partial \bar{p}}{\partial z} = -\bar{\rho} g H, \tag{4}$$

$$\frac{\partial}{\partial s}(c\bar{v}) + \frac{\partial}{\partial z}\left(\frac{a}{H}\bar{w}\right) = 0, \tag{5}$$

$$\frac{\partial \bar{T}}{\partial t} + \frac{\partial}{\partial s}\left(\frac{c\bar{v}}{a}\bar{T}\right) + \frac{\partial}{\partial z}\left(\frac{\bar{w}}{H}\bar{T}\right) = \frac{\partial}{\partial s}\left(\frac{c^2 K_H}{a^2}\frac{\partial \bar{T}}{\partial s}\right) + \frac{\partial}{\partial z}\left(\frac{K_V}{H^2}\frac{\partial \bar{T}}{\partial z}\right), \tag{6}$$

$$\frac{\partial \bar{S}}{\partial t} + \frac{\partial}{\partial s}\left(\frac{c\bar{v}}{a}\bar{S}\right) + \frac{\partial}{\partial z}\left(\frac{\bar{w}}{H}\bar{S}\right) = \frac{\partial}{\partial s}\left(\frac{c^2 K_H}{a^2}\frac{\partial \bar{S}}{\partial s}\right) + \frac{\partial}{\partial z}\left(\frac{K_V}{H^2}\frac{\partial \bar{S}}{\partial z}\right), \quad (7)$$

$$\bar{\rho} = \rho_*[1 - \alpha(\bar{T} - T_0) + \beta(\bar{S} - S_0)], \quad (8)$$

where $s = \sin\phi$, $c = \cos\phi$, ϕ is the latitude, and z is the nondimensional vertical coordinate, increasing from -1 at the bottom to 0 at the top; u, v, and w are the horizontal and vertical velocity components; T, S, ρ, and p denote the temperature, salinity, density, and pressure; $\rho_* = 1027.79$ kg m^{-3}, $T_0 = 4$°C, $S_0 = 35$ ppt, $\alpha = 0.223$ kg m^{-3} K^{-1}, and $\beta = 0.796$ kg m^{-3} ppt^{-1}; Ω and a are the angular velocity and radius of the earth, g is the acceleration due to gravity, and $A = 10^{-4}$ m^2 s^{-1} is a constant vertical eddy viscosity. The zonally averaged east–west pressure gradient,

$$\frac{\Delta p}{\Delta \Lambda} = \frac{p(\lambda_E, s, z) - p(\lambda_W, s, z)}{\lambda_E - \lambda_W}, \quad (9)$$

cannot be determined from (2)–(8), and an additional parameterization is required to close the system. This will be discussed in section 2c.

We assume that $\overline{\alpha\beta}$ can be reasonably approximated by $\bar{\alpha} \cdot \bar{\beta}$ for any quantities α and β in (6) and (7). The major physical effect neglected by making this approximation is the horizontal heat and salt transports due to gyre circulation. In the absence of wind stress, the gyre circulation is weak, and this is a good approximation. Even with wind stress included, there is some support for this approximation. Experiments with general circulation models of the ocean (Meehl et al. 1982; Bryan 1987) and a coupled atmosphere–ocean GCM (Manabe and Stouffer 1988) suggest that the northward transport of heat in the Atlantic under present conditions is dominated by the meridional overturning or thermohaline circulation. Based on these results we neglect the meridional transport due to gyres. This may not be a good approximation when the flow exhibits a very weak and shallow thermohaline circulation.

Boundary conditions have to be specified at the top and the bottom of the ocean, as well as at the northern and southern walls of the basin. At the ocean surface, the fluxes of momentum, heat, and salt are continuous, and the vertical velocity vanishes in a rigid-lid formulation. For a buoyancy-driven ocean we have

$$\rho_* A(u_z, v_z) = 0, \quad w = 0, \quad (10a\text{–}c)$$

$$-\frac{K_V}{H}(T_z, S_z) = (Q_H, Q_S), \quad (10d,e)$$

where the overbars are here and henceforth dropped; Q_H is the flux of heat from the ocean to the atmosphere (note the sign convention, whereby positive fluxes are strictly upward). For ocean-only runs Q_H represents a heat flux due to Newtonian cooling, namely,

$$Q_H = \frac{H\Delta z}{\tau_H}(T - T^*), \quad (11)$$

where Δz is the nondimensional depth of the top grid box, T^* is a prescribed relaxation temperature, and τ_H a relaxation time scale for heat. Likewise, the salt flux is given by one of the following equations:

$$Q_S = \begin{cases} \dfrac{H\Delta z}{\tau_S}(S - S^*) & (12a) \\ Q_S^*. & (12b) \end{cases}$$

In (12a), S^* and τ_S are the relaxation salinity and time scale, respectively; whereas in (12b), Q_S^* is a fixed salt flux, which may be diagnosed from a previous calculation. The use of (11) in conjunction with (12b) is a standard procedure for climate models and represents the case of *mixed boundary conditions* (Welander 1986). They account for the fact that sea surface temperature influences the heat flux (sensible, longwave, and latent); sea surface salinity, on the other hand, has no instantaneous effect on the salt flux (precipitation–evaporation).

At the ocean bottom a no-stress boundary condition is applied, and we assume no material or energy fluxes through the bottom. This leads to

$$A(u_z, v_z) = 0, \quad w = 0, \quad (13a\text{–}c)$$

$$(T_z, S_z) = 0. \quad (13d,e)$$

At the southern ($s = s_0$) and northern ($s = s_1$) basin walls, no-flux conditions on T and S imply

$$\frac{\partial}{\partial s}(T, S) = 0. \quad (14)$$

Note that for the southern and northern walls no conditions on the velocity fields are imposed. No flux through these boundaries follows from (14) by use of the equation of state. From it we have $\partial\rho/\partial s = 0$ at s_0 and s_1, and hence $\partial p/\partial s$ is depth independent. With the parameterization chosen for Δp (see section 2c), this implies $\Delta p = 0$. Thus, from (2), (3), (10a,b), and (13a,b) it is apparent that $u = v = 0$.

b. *Determination of the velocity field*

In solving equations (2)–(14), it is convenient to make use of (5) and introduce the meridional overturning streamfunction ψ defined by

$$v = -\frac{1}{Hc}\frac{\partial \psi}{\partial z}, \quad w = \frac{1}{a}\frac{\partial \psi}{\partial s}. \quad (15)$$

Differentiating (3) with respect to z, substituting the

resulting expression for u_z into (2), and then using (15) to eliminate v, we obtain

$$\psi_{zzzzz} + (s/\tilde{A})^2\psi_z = \frac{H}{2\rho_* a\Omega\tilde{A}}\left(gHc^2\frac{\partial^2\rho}{\partial s\partial z} - (s/\tilde{A})\frac{\Delta p}{\Delta\Lambda}\right), \quad (16)$$

where $\tilde{A} = A/(2\Omega H^2)$, and (4) has been used to eliminate p_z. Equation (16) is a restatement of the zonal momentum equation (2).

Boundary conditions for ψ are determined from (10a,b,c) and (13a,b,c) by eliminating u and u_z with the use of (3) to give

$$\psi_{zzzz} = \frac{gH^2c^2}{2\rho_*\tilde{A}\Omega a}\frac{\partial\rho}{\partial s}, \quad (17a)$$

$$\psi_{zz} = 0, \quad (17b)$$

$$\psi = 0, \quad (17c)$$

which apply at both $z = 0$ and $z = -1$, yielding six boundary conditions. From (16) only five boundary conditions on ψ can be satisfied, and hence one of the conditions (17) must be redundant for consistency. Indeed, integrating (16) over the water column and using (17a,c), any one of the four conditions associated with (17a,c) may be shown to be redundant with respect to the remaining equations.

To solve (16) we first note that the boundary layers at the surface and bottom have thicknesses of order $(\tilde{A}/s)^{1/2} \approx$ O(1 m). Standard boundary-layer techniques may thus be applied to show that, for a grid that does not resolve the top and bottom boundary layers, the streamfunction ψ at interior grid points is given by

$$\psi(s, z) = \frac{H}{2\rho_* a\Omega s^2}\left(\tilde{A}gHc^2\frac{\partial\rho}{\partial s} - s\int_{-1}^{z}\frac{\Delta p}{\Delta\Lambda}\,dz\right), \quad (18)$$

and $\psi(s, 0) = \psi(s, -1) = 0$. The first term on the rhs of (18) represents the frictionally induced flow associated with vertical gradients in the internal stress Av_z; while the second term is the geostrophic flow due to the east–west component of the pressure gradient. A parameterization of this pressure gradient in terms of known quantities eventually allows us to calculate ψ. This will be presented in the following section.

Finally, it is noted that (18) does not hold at the equator. In the present study the grid has always been chosen such that ψ need not be determined at $s = 0$. In global runs the central grid cell straddles the equator, while in hemispheric runs we set $\psi = 0$ at the equator as a boundary condition.

c. *Parameterization of the east–west pressure gradient*

The model formulation can only be completed if Δp in (18) is linked with the other variables in the model. This problem has been recognized previously by MWW, but their resolution is different from ours.

One limiting case is an ocean that is unbounded (and hence cyclic) in the east–west direction. For this case $\Delta p = 0$, and it follows from (2) and (3) that the zonally averaged north–south flow reduces to that associated with stresses acting on the nearly geostrophic zonally averaged east–west flow. The meridional circulation is thus very weak and a poor approximation to that in a zonally bounded basin. This case is not relevant to the time scales of interest here, for which advection by the meridional circulation is critically important.

A second tractable limiting case is an ocean basin that is so narrow that the east–west flow is negligible. Setting $\bar{u} = 0$ in (2) and (3), one finds

$$\frac{A}{H^2}v_{zz} = \frac{A}{2\rho_* H^2 ac\Omega s}\frac{\Delta p_{zz}}{\Delta\Lambda} = \frac{c}{\rho_* a}\frac{\partial p}{\partial s}. \quad (19)$$

Again, this allows us to determine $\Delta p/\Delta\Lambda$. In this limit $\partial p/\partial s$ drives the meridional circulation directly rather than being largely balanced by the Coriolis force, which is associated with the east–west flow in the case of a wider basin. Equation (19) is thus not applicable to wider basins. One possible solution to this problem is to artificially increase the value of A so that v is reduced to an acceptable range. This yields the parameterization considered by MWW.

For an ocean of intermediate width, a relation between the two components of the pressure gradient is not immediately apparent. The following argument, which is admittedly somewhat ad hoc, is useful in suggesting an appropriate relationship. Consider the momentum equations (2) and (3) with eddy diffusion neglected in (2) and replaced by linear damping $-\mu\bar{v}$ in (3) (Killworth 1985). Ekman layers are clearly excluded by this formulation; inclusion of wind stress would require additional considerations. Solving for $\Delta p/\Delta\Lambda$,

$$\frac{\Delta p}{\Delta\Lambda} = -2\epsilon sc^2\frac{\partial p}{\partial s}, \quad (20)$$

where

$$\epsilon = \frac{\Omega}{\mu}\left(1 - \frac{u}{u_g}\right) \quad (21)$$

and the zonally averaged geostrophic velocity u_g is defined by

$$u_g = -\frac{c}{2\rho_* as\Omega}\frac{\partial p}{\partial s}. \quad (22)$$

For a narrow basin $u/u_g \approx 0$, and ϵ is the ratio of the damping to the inertial time scale. Even for the large damping rate of $\mu^{-1} = 3$ days (Killworth 1985), this limit gives $\epsilon \approx 20$. In a realistic ocean basin, which is many internal Rossby radii across, we expect that u

will be almost equal to u_g, so ϵ would be greatly reduced; ϵ is determined by the slight deviations from geostrophy.

Although we expect ϵ to be generally positive, it may vary spatially. Nevertheless, as a closure we have chosen to investigate the parameterization (20) with ϵ simply fixed at a constant value. Note that this parameterization yields reasonable results at the equator as well as at the poles. Near the equator $\Delta p/\Delta\Lambda \sim s\partial p/\partial s$ indicates proportionality to f, the Coriolis parameter. The meridional velocity v stays finite at the equator without incorporation of new dynamics. At the poles $\Delta p/\Delta\Lambda \sim c^2\partial p/\partial s$ tends to zero. Likewise, $v \sim c\partial p/\partial s$ tends to zero at the poles.

It is of interest to consider the parameterization (20) with the geostrophic approximation to v. This yields

$$-\frac{\Omega}{\epsilon}v = \frac{c}{\rho_* a}\frac{\partial p}{\partial s}. \tag{23}$$

This relation is equivalent to (19) with Rayleigh damping instead of eddy diffusion. Parameterization (23) is consistent with those used by Stommel (1961), Welander (1986), and Rooth (1982), but is inconsistent with the Fickian diffusion (Av_{zz}) used by MWW. The large value of A used by MWW, which is required to compensate for the lack of a Coriolis term, eliminates any possibility of return flow being carried in a relatively thin surface layer. The presence of these boundary layers is central to the formulation here and represents an extension of the earlier model.

To test the validity of (20) and estimate an appropriate value for ϵ, two different approaches were used. Initially, we performed a series of model runs with ϵ varying and all other model parameters fixed. The details of some of these runs are discussed in section 4a. From this series of runs it was determined that, for the model parameters considered, a value of $\epsilon = 0.5$ yielded a reasonable meridional overturning rate of order 10 Sv (1 Sv $\equiv 10^6$ m^3 s^{-1}).

A more stringent test of the form of (20) and an estimate of ϵ based on more realistic forcing was obtained using results from the three-dimensional Bryan–Cox OGCM study by Weaver and Sarachik (1990). They determined a steady-state circulation in a 60° wide hemispherical basin by restoring surface temperature and salinity to zonally averaged Levitus (1982) data and applying a realistic wind stress. This steady state (Weaver and Sarachik 1990, Fig. 4b) was integrated for another 2630 surface years with no wind forcing, and the resulting fields were used in the calculations discussed below.

Unfortunately pressure is not a standard output from the OGCM, so (20) was differentiated with respect to z (thus replacing p by ρ) and integrated from the surface downward to obtain the relation

$$\int_0^z \frac{\Delta\rho}{\Delta\Lambda}\,dz = -2\epsilon sc^2\int_0^z \frac{\partial\rho}{\partial s}\,dz, \tag{24a}$$

or equivalently

$$\frac{\Delta(p-p_s)}{\Delta\Lambda} = -\epsilon\left(2sc^2\frac{\partial}{\partial s}(p-p_s)\right). \tag{24b}$$

Values of the integrals in (24a) were determined at each latitude and each vertical level of the model. Finally, at each level all but the three northern and southern (6° latitude) values were used to obtain a least squares estimate of ϵ and the correlation coefficient between the left and right sides of (24b). Inclusion of the six neglected cells would not greatly influence the least squares estimates of ϵ, but it would reduce the correlation coefficient. Figure 1 shows relation (24b) at 570-m (○) and 2135-m (●) depth; the estimated ϵ are 0.30 and 0.27, respectively. The estimates of ϵ (○) and correlation coefficients (●) as functions of depth are displayed in Fig. 2. Below 500 m a constant value of $\epsilon \approx 0.3$ is appropriate. High values of the correlation coefficients indicate that the latitudinal structure of the relationship between the pressure gradient components is reasonably approximated by (20).

The apparent degradation toward $z = 0$ in Fig. 2 is somewhat misleading. Recalling that results were obtained from a run with surface values relaxed to zonally averaged data, it is noted that, since $\Delta\rho \to 0$ at $z = 0$, ϵ must tend to zero there. Vertical diffusion will convey this effect to deeper levels, so we expect ϵ to decrease smoothly to zero at $z = 0$ as observed. Since both left and right sides of (24) vanish at $z = 0$, it is also not

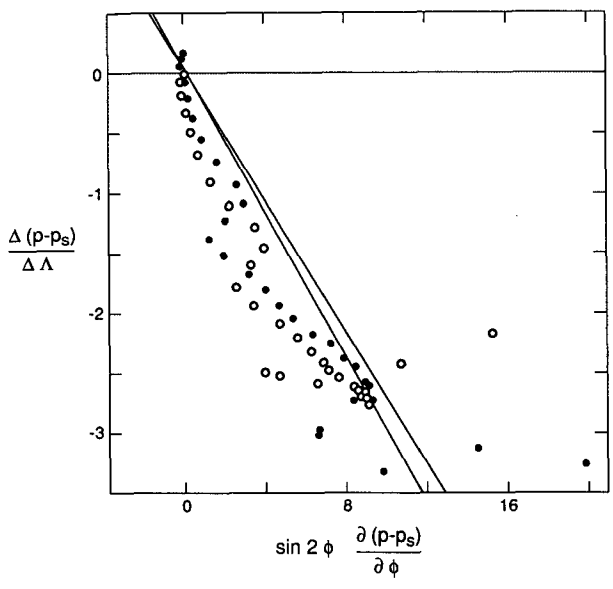

FIG. 1. The relation between the lhs and rhs of (24b) determined from the steady-state circulation of the Bryan–Cox OGCM in a hemispheric basin with no wind stress (Weaver and Sarachik 1990). The values are plotted for 27 latitudes from 60°S to 5°S at depth 570 m (○) and 2135 m (●); scales are multiplied by 10^{-3}. The slopes and correlations are −0.30, 0.65 for (○) and −0.27, 0.78 for (●).

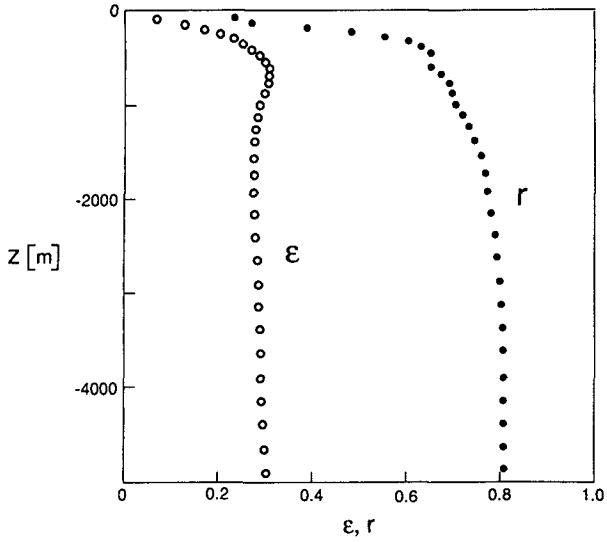

FIG. 2. Constant of proportionality ϵ and correlation of the linear fit as functions of depth. Correlations are of order 0.8 for the main part of the water column; ϵ increases over the first 500 m and is nearly constant at $\epsilon \approx 0.3$ below.

surprising to find a low correlation coefficient there: local shears should not be expected to be accurately modeled by (24).

Finally, it is noted that if the transport carried below 500 m is accurately estimated using (24), then the net transport above 500 m must also be accurately determined since the sum over the two regions vanishes. Thus, although details may be poorly represented, (24) should give a useful approximation to the overall vertical structure of the meridional circulation throughout the water column.

3. Numerical solution procedure

A solution of Eqs. (2)–(7) is conveniently achieved by use of the meridional overturning streamfunction given by (15). The diagnostic equation for the streamfunction (18) and the prognostic advection–diffusion equations (6) and (7) for temperature and salinity are solved on a uniform grid spanning the (s, z) coordinates with N vertical layers, each containing M grid boxes. The flux fields are calculated on the box walls, whereas the volume fields are taken centered. For $N = 20$, the top layer of 250 m is represented only by its average temperature and salinity fields. This is not satisfactory for the calculation of surface fluxes, so a linear extrapolation of T and S is used to estimate surface values.

The first step of the numerical procedure is to calculate the density gradients. Centered differences are used to estimate values at interior cell boundaries. Normal derivatives vanish at the bottom, north, and south boundaries, and values at the surface are consistent with the linear extrapolation of T and S to the surface. Values within cell boundaries are obtained by linear interpolation. The meridional overturning transport is then diagnosed in a vertical column using the imposed boundary conditions. With the velocity field known, the advection–diffusion equations (6) and (7) are solved by applying the numerical scheme of Fiadeiro and Veronis (1977) for calculation of the fluxes across cell boundaries. Simple forward differencing is used in the time domain. With T and S determined, ρ is obtained from (8). A nondiffusive convection scheme is used to ensure complete mixing of unstable water masses after a finite number of iterations.

4. Spinup and test runs

The standard procedure of ocean spinup is applied. Basic model parameters are given in Table 1. Integration starts from an ocean at rest with uniform temperature $T = 7°C$ and salinity $S = 35$ ppt. The circulation is set up by thermal and haline surface forcing. At the ocean surface T and S are relaxed to specified values T^* and S^* on a time scale of 100 days. Following MWW, we use the analytic forms:

$$T^* = (1 + \cos(\pi s)) \times 12.5°C, \quad (25a)$$

$$S^* = (36 + \cos(\pi s)) \text{ ppt}. \quad (25b)$$

With these values, the temperature effect dominates the equator-to-pole density difference by about a factor of three compared to the salinity effect, so the resulting meridional circulation is downwelling at the poles. Although (25a,b) are chosen to be qualitatively consistent with observations, they are obviously crude. To obtain a meridional overturning rate of order 10 Sv, we have taken $\epsilon = 0.5$ throughout the remainder of this paper.

The system is near equilibrium after a few hundred years, but the integration is carried out to 5050 yr. The final equilibrium is shown in Fig. 3. The two-cell circulation is in qualitative agreement with the results of Bryan (1986), MWW, and Weaver and Sarachik (1991a). A conspicuous contrast to the circulation of MWW is that the meridional flow feeding the region of deep-water formation is surface trapped (Fig. 3a). This is a phenomenon that also occurs in the zonal

TABLE 1. Basic model parameters.

Parameter	Hemispheric	Global
ϕ_0	0°	80°S
ϕ_1	80°N	80°N
H	5000 m	5000 m
$\Delta\Lambda$	60°	60°
M	10	21
N	20	20
K_V	0.4×10^{-4} m^2 s^{-1}	0.4×10^{-4} m^2 s^{-1}
K_H	10^3 m^2 s^{-1}	10^3 m^2 s^{-1}
A	10^{-4} m^2 s^{-1}	10^{-4} m^2 s^{-1}

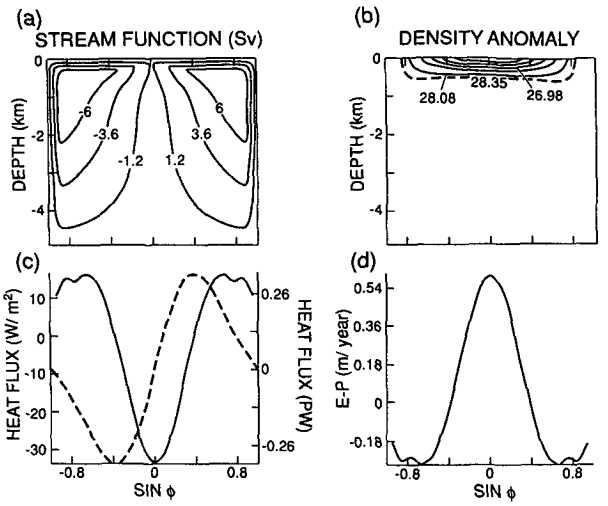

FIG. 3. Contours of the meridional overturning streamfunction in Sv (1 Sv ≡ 10^6 m^3 s^{-1}) (a) and density anomaly in kilograms per cubic meter (b). The steady state in a global basin under restoring boundary conditions consists of two cells with deep-water formation at both high latitudes. Meridional heat flux (dashed) in PW (1 PW = 10^{15} W) and vertical surface heat flux (solid) in watts per square meter (c) are symmetric about the equator. The vertical surface salt flux is given as an equivalent freshwater flux E–P in m yr^{-1} (d).

averages of three-dimensional OGCMs and suggests that the model here reproduces the qualitative features of the meridional deep circulation fairly realistically.

From the equilibrium state described above, the vertical surface salt flux Q_S^* was diagnosed (Fig. 3d) and is used as the surface boundary condition on salt (12b) henceforth. The temperature field was still relaxed to (25a) forming the usual mixed boundary conditions. Starting from this steady state, three experiments were performed under identical boundary conditions but with different initial salinity anomalies added to the surface layer: no salinity anomaly added, 0.2 ppt added north of 38°N, and −0.2 ppt added south of 38°S. Integration was continued for an additional 2500 years.

The results were generally consistent with previous studies (MWW; Bryan 1986), and details are not shown here. The most important conclusion is that the symmetric circulation in Fig. 3 is unstable under mixed boundary conditions. In all three experiments a new steady state was established, that consisted of a single cell with deep-water formation in high latitudes. Figure 4 shows the steady state established at the end of the run in which no salinity anomaly was added: the steady state for the other two runs was essentially identical but reflected about the equator, as expected from the initial anomalies. In each case, the transition to a single-cell circulation occurred, once initiated, over a period of order 100 years.

The instability of the direct symmetric circulation demonstrated here and by MWW contrasts with the stability of the direct symmetric circulation determined by Welander (1986) using a simple three-box model with no vertical resolution. To illustrate the origin of this difference, consider the consequence of adding some salt to one of the polar cells in Welander's model. The density of the polar cell increases so that the advective exchange of water between the polar and equatorial boxes increases. However, the decreased salinity contrast between the boxes causes the advective exchange of salt to decrease. Consequently, the forcing associated with Q_S^* dominates that due to advection and reduces the salinity toward its original value, resulting in a stable equilibrium. In models with multiple vertical levels the situation is different. The addition of salt to the surface cell of the polar box still increases the advective exchange of water, but now the salinity of the deep water in the polar box is unchanged so that there is no immediate change in the salinity of the water being exchanged between high and low latitudes. The increased circulation thus leads to a further increase in polar salinity. The perturbation is enhanced, leading to instability of the symmetric circulation.

5. Thermohaline catastrophe and subsequent evolution

a. Hemispheric basin

We now study the present model in the restricted geometry of a hemisphere to reexamine the results of Marotzke (1989). The basin is 5000 m deep and extends from 0° to 80°N with 60° angular width; a 10 (horizontal) × 20 (vertical) grid is chosen. The steady state under restoring boundary conditions is shown in Fig. 5, from which a control run and a perturbation experiment continue, both under mixed boundary conditions.

For the control run, the adjustment after switching boundary conditions is minor, although the maximum transport increased by about 15% over that in Fig. 5. This increase occurred abruptly about 100 years after the change in boundary conditions, and the transients, whose initial peak-to-peak amplitude were about 1 Sv,

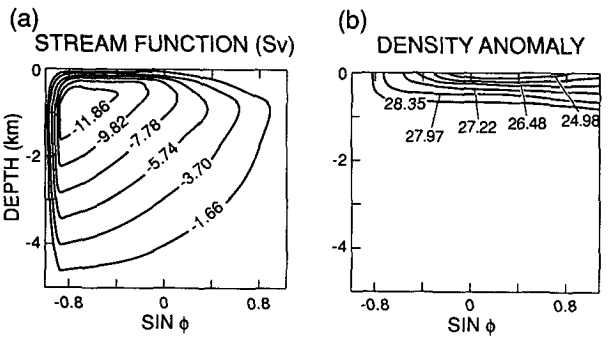

FIG. 4. Contours of the meridional overturning streamfunction (a) and density anomaly (b) of the steady state in a global basin achieved after switching to mixed boundary conditions with no salinity anomaly added (t = 7400 yr).

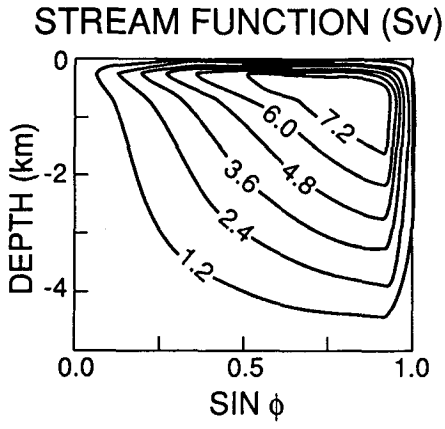

FIG. 5. Steady-state overturning streamfunction for a hemispheric basin under restoring boundary conditions (t = 5050 yr). The change to mixed boundary conditions causes only minor adjustments.

had become negligible a few hundred years later. This shows that there is a stable equilibrium under the mixed boundary conditions, which is very similar but not identical to that under the restoring boundary conditions.

The situation is different when a small negative salinity anomaly of 0.1 ppt is added north of 36°N. Figure 6a shows the circulation and density fields 600 years after the freshening of the region of deep water formation. The positive circulation has collapsed due to the process described by Bryan and now consists of a shallow, indirect cell located at low latitudes. The state found here is in qualitative agreement with the three-dimensional results presented by Marotzke (1989). Analysis of the surface heat flux reveals a net uptake of heat through the surface, implying subsequent adjustments. Twenty thousand years later the circulation had deepened to about twice the depth seen in Fig. 6a, and the associated transport had decreased by about a factor of 2. The most striking change, however, is due to the heat input during the intervening years, which causes the deep ocean to warm up by some 13°C. The surface-to-bottom density contrast decreases from 2.4 kg m^{-3} at t = 8000 yr to 0.2 kg m^{-3} 20 000 years later.

The consequence of this long-term process is the dramatic event at t = 28 620 yr (Fig. 7a) when massive convective mixing at high latitudes sets in and accelerates the circulation to a maximum of 380 Sv (Fig. 6b). The violent circulation is basinwide and causes major rearrangements in the temperature and salinity fields. The downwelling in high latitudes effectively releases all the heat taken up during the previous millenia at rates exceeding 400 W m^{-2}. Immediately after the period of very rapid changes, there is a period of about 2000 years when the circulation is variable but generally similar to that illustrated in Fig. 5. This state eventually collapses again, returning to a state similar to that shown in Fig. 6a. The above process repeats itself two more times during the next 50 000 years of integration (Fig. 7a shows two cycles of this process).

These so-called *flushes* (transports exceeding 200 Sv) were first reported by Marotzke (1989) in both two- and three-dimensional hemispheric ocean models. The three-dimensional OGCM of a global basin by Weaver and Sarachik (1991a) shows a sequence of less violent flushes (50+ Sv) recurring on a time scale of 200 to 1000 years, which eventually give way to a remarkably steady state. This time scale hints at a process different from vertical diffusion important in Marotzke (1989) and the experiments presented here. In an additional run of our two-dimensional model (not shown) with K_V increased from 0.4 × 10^{-4} m^2 s^{-1} to 10^{-4} m^2 s^{-1}, the ocean state evolved up to and through the first flush essentially as described above, except that the diffusive stage had shorter duration, as expected. After the flush, however, the period of variable transport, which previously lasted for 2000 years, now lasted for the remainder of the model run (15 000 years). Apparently the increased vertical diffusion was sufficient to prevent the complete collapse of the circulation. Clearly, the sensitivity of model results to the rather uncertain choice of vertical diffusion warrants further investigation in both two- and three-dimensional models.

b. Instability of the purely diffusive steady state

When the circulation is collapsed to the state in Fig. 6a, advective and convective processes are no longer important; instead, the evolution is dominated by diffusion. As will be seen below, both T and S in the deep ocean will tend to the average surface values with neg-

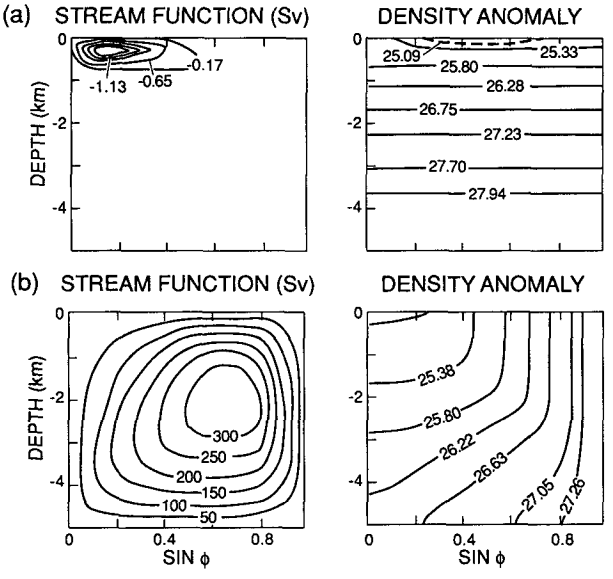

FIG. 6. Overturning streamfunction and density anomaly at t = 8000 yr (a) and t = 28 620 yr (b). The state of (a) is diffusion dominated leading to the violent overturning (>300 Sv) in (b).

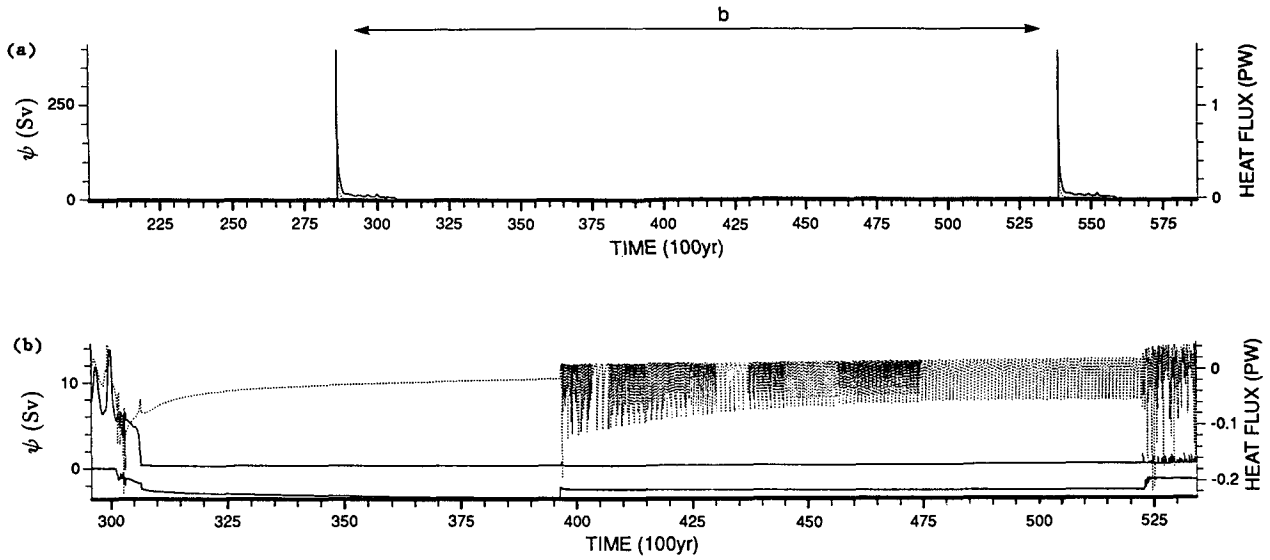

FIG. 7. Evolution of the maximum streamfunction shows two flushes in the hemispheric model run. A deep circulation oscillates in strength for about 2000 years after the first flush and finally collapses to a surface intensified negative circulation (a). Maximum and minimum streamfunction (solid) and total surface heat flux (dotted) evolve smoothly for about 9000 years after the collapse (b), then low-latitude instability sets in at t = 39 500 yr. This leads eventually to larger perturbations (t = 52 500 yr), which trigger the high-latitude instability causing the flush at t = 53 850 yr.

ligible latitudinal structure. This leads to a stabilization with respect to temperature and a destabilization with respect to salinity of the equatorial water column. The effects are reversed in the polar water column.

To obtain a quantitative understanding of the important processes, we consider a simple diffusive model. Let y and z be dimensional coordinates for latitude and depth, and consider the T and S fields corresponding to a diffusive equilibrium governed by

$$K_H T_{yy} + K_V T_{zz} = 0, \tag{26a}$$

$$K_H S_{yy} + K_V S_{zz} = 0, \tag{26b}$$

in a basin of depth H and length L. Applying mixed boundary conditions at the surface $z = 0$ of the form

$$T = T_0\left(1 + \cos\frac{\pi y}{L}\right), \tag{27a}$$

$$K_V S_z = F_0 \cos\frac{\pi y}{L}, \tag{27b}$$

no-flux conditions at the basin walls, and defining

$$\kappa \equiv \frac{\pi}{L}\left(\frac{K_H}{K_V}\right)^{1/2}, \tag{28}$$

the steady-state solutions are given by

$$T = T_0\left(1 + \cos\left(\frac{\pi y}{L}\right)\frac{\cosh\kappa(z+H)}{\cosh\kappa H}\right), \tag{29a}$$

$$S = S_0 + \frac{F_0}{\kappa K_V}\cos\left(\frac{\pi y}{L}\right)\frac{\cosh\kappa(z+H)}{\sinh\kappa H}. \tag{29b}$$

For $K_H = 10^3\ \mathrm{m^2\ s^{-1}}$, $K_V = 0.4 \times 10^{-4}\ \mathrm{m^2\ s^{-1}}$, $L = 10^7$ m, and $H = 5 \times 10^3$ m, the vertical decay scale $1/\kappa$ is about 400 m. Also, $\kappa H \approx 12.5$, and below a thousand meters the temperature and salinity are nearly uniform and close to the average surface values T_0 and S_0. For the linear equation of state

$$\rho = \rho_0(1 - \alpha(T - T_0) + \beta(S - S_0)), \tag{30}$$

the criterion for stability of this diffusive equilibrium is

$$\alpha T_z > \beta S_z, \tag{31}$$

which becomes, using (29),

$$R > 1, \quad \text{for} \quad 0 < y < L/2,$$

$$R < 1, \quad \text{for} \quad L/2 < y < L, \tag{32}$$

where

$$R = \frac{\pi(K_V K_H)^{1/2}\alpha T_0}{L\beta F_0}. \tag{33}$$

Instability is therefore *inevitable* and occurs either at low latitudes ($R < 1$) or at high latitudes ($R > 1$). The solution (29) will thus never be realized. Note that R is the ratio of the surface buoyancy fluxes associated with temperature ($\sim\alpha\kappa K_V T_0$) and salinity ($\sim\beta F_0$). The condition (32) states that the stabilizing effect of temperature (salinity) must dominate at low (high) latitudes for the density stratification to remain stable.

The evolution following the initiation of convective instability is different for these two cases. For the case $R < 1$, low-latitude convection reduces both salinity and temperature at the surface with the reverse but weaker effects at depth. The strong feedback on temperature quickly removes the surface temperature anomaly leaving a stable stratification due to the reduced surface salinity. The system subsequently evolves again toward the unstable state, and the process repeats on a time scale governed primarily by surface exchange and diffusive processes. In this case, convective mixing represents a relatively minor modification to the diffusive equilibrium.

A high-latitude convective instability, on the other hand, evolves differently as observed in the experiments above and earlier by Marotzke (1989). Again, temperature anomalies are efficiently removed under the restoring conditions. Surface salinity, however, is increased by convection yielding an even less stable situation. This accelerates vertical mixing, which brings warmer waters up to the surface. As a consequence of the restoring condition on temperature, heat is lost in high latitudes at an unrealistically large rate. The cooling causes a rapid increase of the density starting the violent overturning of Fig. 6b. Initially, only the high-latitude density is affected, so the circulation is confined to this region. However, relatively saline water is carried into adjacent surface regions triggering instability there also. The combination of very strong advection and subsequent convection homogenizes the northern half of the domain from top to bottom over a period of order two years. This rapid evolution is retarded in the southern half of the domain where the importation of deep water to the surface layer actually reduces the surface salinity, hence increasing the vertical stability of the water column. The influence of the dramatic changes occurring at higher latitudes is nevertheless communicated to the equatorial region through the slower process of horizontal diffusion.

The model clearly exhibits both forms of instability. Figure 7b shows a close-up of the evolution of the maximum and minimum streamfunction and the basin-integrated surface heat flux (in PW) during the diffusion-dominated state between the two flushes seen in Fig. 7a. Low-latitude instability sets in at $t = 39\ 500$ yr and results in a vacillating surface heat flux over the next 12 000 years. A slight reduction in transport occurs at this time. Repeated low-latitude convection and diffusion slowly increases the deep ocean temperatures, thus, shifting the system toward a high-latitude instability. At about 52 300 years, the evolution becomes even more chaotic, and the transport is reduced further. Eventually, the high-latitude instability occurs as a flush. The maximum streamfunction amplitude reaches about 400 Sv, indicating the major rearrangements discussed above. We conclude that low-latitude convection together with diffusion, operating over long time scales, can trigger a high-latitude instability.

c. *Global basin*

Two experiments investigating the model behavior in one global basin are presented in this section. In the first experiment, we start from the steady-state two-cell circulation of Fig. 3. Mixed boundary conditions are applied, and a weak negative salinity anomaly of 0.2 ppt is added north of 36°N, as well as south of 36°S. The circulation collapses in both hemispheres, each of which exhibits fields as displayed in Fig. 6a. The initial response to the anomaly is identical to two hemispheres back-to-back with an equatorial wall. For about 3800 years no changes are apparent. From about $t = 8800$ yr to $t = 11\ 800$ yr, small, symmetric deviations with amplitudes of order 0.5 Sv or less in transport are evident, and near $t = 11\ 800$ yr major transient adjustments begin. By $t = 13\ 500$ yr (8500 yr after the initial perturbation) the new state consists of a single, shallow cell of 4 Sv located slightly off the equator (Fig. 8a). Further evolution of this state is discussed below.

In the second experiment we start from the stable one-cell circulation shown in Fig. 4 (reflected about the equator) and add a 2-ppt negative salinity anomaly north of 36°N only. The anomaly immediately causes a shallowing of the one-cell circulation, and the pattern shown in Fig. 8a is established within 50 years. The subsequent evolution of the two experiments is essentially identical. During the next 22 000 years diffusion dominates, and as in the hemispheric experiment, low latitude convection occurs, as evidenced by the vertical isopycnals near $s = 0.4$ in Fig. 8a. Due to vertical dif-

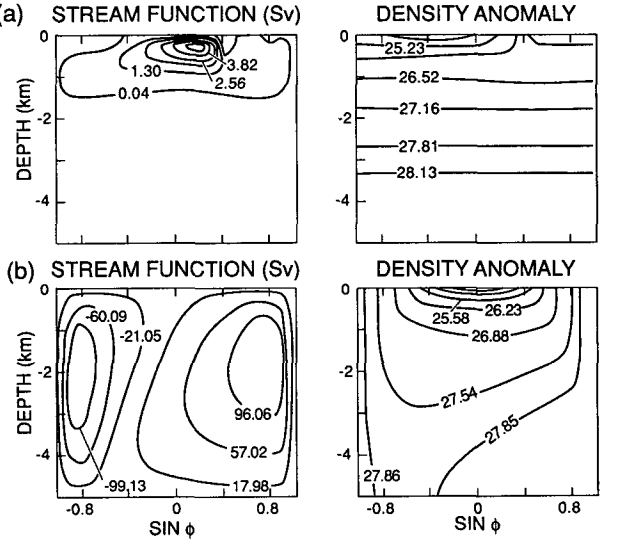

FIG. 8. (a) The deep circulation in a global model after adding fresh water in both high latitudes to the state of Fig. 3a or, alternatively, adding fresh water only to the high northern latitudes of Fig. 4 (reflected about the equator). Both perturbations lead to the collapsed state; $t = 13\ 500$ yr. (b). Violent convective overturning starts with a northern cellfirst, a southern cell is set up later; $t = 31\ 705$ yr.

fusion, the deep-ocean temperature increases from 2° to 16°C, and the water column stability is weakened accordingly. The circulation at the end of this diffusive period is roughly doubled in strength and depth compared to that in Fig. 8a, but is still confined to the near-surface region. A few years later, convection starts at high northern latitudes, and a flush begins. As in the hemispheric case a single overturning cell develops in high northern latitudes with a maximum transport of ~360 Sv. Heat is released at a rate of ~450 W m^{-2}, producing cold water that is mixed down to the deep ocean. At the same time, warm bottom water upwells in the Southern Hemisphere increasing the heat flux to the atmosphere. This heat loss initiates convection at high southern latitudes, and a negative circulation develops there (Fig. 8b). The transition passes a nearly symmetric state, and both cells then decay over the next 100 years. The southern cell eventually disappears, and the *stable* one-cell circulation develops (Fig. 4, reflected about the equator). Unlike in the hemispheric basin, where several successions of flushes and collapsed states were observed, no further evolution of the one-cell circulation was found in the global basin.

6. Concluding remarks

Several experiments in both hemispherical and global ocean basins have been performed with the present zonally averaged ocean model. The results of MWW and Marotzke (1989) were generally confirmed. In the geometry of a hemisphere the steady states under restoring and mixed boundary conditions were found to be quantitatively similar. For surface forcing of the form (25), deep water is formed in high latitudes, and upwelling occurs at low latitudes. When switched to mixed surface boundary conditions, minor adjustments happen, and a new state is established that is stable to small perturbations. The meridional flow feeding the region of deep-water formation in the present model is surface trapped. This also compares favorably with the zonal averages of three-dimensional OGCMs (Bryan 1986; Marotzke 1989; Weaver and Sarachik 1990).

The two-cell thermohaline circulation obtained in a global ocean under restoring boundary conditions is, as expected, not stable upon a switch to mixed boundary conditions. A spontaneous transition to a one-cell circulation has already occurred by 100 years after the switch. This time is considerably shorter than the one reported by MWW, but additional results show that it is strongly parameter sensitive. Application of negative or positive salinity anomalies affects the timing of the transition phase as different feedback mechanisms are operating (Bryan 1986). The resulting steady state is identical for the three cases. The important point is that the symmetric circulation is unstable and is not expected to occur in reality.

Long time integrations over many tens of thousands of years were performed for both hemispheric and global basins. In the hemisphere, a negative anomaly causes a breakdown of the deep circulation changing it to a weak, surface-trapped circulation. The deep ocean is increasingly diffusion dominated. As a result of a steady influx of heat through the ocean surface, stability of the high latitude water column is gradually lost. Violent convective overturning sets in, and the accumulated heat in the ocean is rapidly released in high latitudes. A basinwide circulation prevails for about 2000 yr, only to collapse once again. This cycle was observed three times and is assumed to be a persistent pattern. Therefore, in the hemispheric basin at least two different modes of circulation under identical forcing could be realized.

Considering the purely diffusive steady state under mixed boundary conditions, we demonstrated that instability is inevitable and can occur either in low or in high latitudes. In the two cases the development is different, in that low-latitude convective mixing has no short-term basinwide effect, whereas high-latitude convective mixing may trigger rapid adjustments in the entire basin.

In a global basin the long-term behavior is different. Cycles of collapsed states and violent convective overturning do not occur. Salinity anomalies caused a collapsed circulation consisting of a weak surface-trapped cell located around the equator. The deep ocean is again diffusion dominated, and after about 22 000 years, convective overturning started. A few hundred years later, the stable one-cell circulation was reestablished. No further evolution of this state is expected.

The results presented here indicate that our zonally averaged model may be a useful tool for the study of some aspects of the dynamics governing the meridional circulation and the associated north–south transports of heat and salt. Even in the present simple form a study of parameter sensitivities would be of interest. Unexpected responses are almost certain to be found; these could be examined in the context of the two-dimensional model and then verified using an OGCM.

The results also suggest some weaknesses of the model. Specification of fixed relaxation temperatures and time scales can clearly lead to unrealistic effects on the meridional circulation. In particular, the strong convective events, during which the ocean loses much of its accumulated heat in a short time, would be damped by an atmosphere that communicates with the ocean surface. This heat warms the overlying atmosphere, decreasing in turn air–sea temperature differences and the associated heat flux. This negative feedback is not included in ocean-only models. It is therefore a worthwhile task to develop a reasonable atmosphere model that will enable us to replace the unrealistic temperature restoring boundary condition. This is done elsewhere (Stocker et al. 1991).

The experiments have also verified that high-latitude processes are critical to the determination of the global

meridional circulation. In the present study the cryosphere is absent. Inclusion of an active high-latitude ice cover would be an important extension. Ice influences both temperature and salinity. The vertical heat flux is reduced in the presence of an ice cover, resulting in a negative feedback for ice growth. On the other hand, melting ice represents a freshwater flux, which could slow down the thermohaline circulation. As a consequence, less heat is carried to high latitudes through the ocean. This, in turn, is a positive feedback for ice growth. The interaction of these two different processes could cause some interesting dynamics of the coupled ocean–ice–atmosphere system.

The present paper emphasizes the significance of the thermohaline circulation of the ocean for natural variability of the climate system and climate change. The eventual goal is to combine the present model with two-dimensional models of the atmosphere and the cryosphere to obtain a realistic and yet inexpensive model suitable for paleoclimatic studies.

Acknowledgments. Professional development leave for DGW, fellowship 82.613.0.88 of the Swiss National Science Foundation awarded to TFS, and research grants from the Canadian Natural Sciences and Engineering Research Council and Atmospheric Environment Service awarded to L. A. Mysak made this study possible. TFS thanks Dr. E. P. Jones for the hospitality and support through a Canadian Panel on Energy Research and Development contract. We enjoyed discussions with Drs. L. A. Mysak and A. J. Weaver, and we thank the latter for making his OGCM data available to us. Two JPO reviewers also provided constructive criticism that improved the presentation of results.

REFERENCES

Broecker, W. S., and G. H. Denton, 1989: The role of ocean–atmosphere reorganizations in glacial cycles. *Geochim. Cosmochim. Acta,* **53,** 2465–2501.

Bryan, F., 1986: High-latitude salinity effects and interhemispheric thermohaline circulations. *Nature,* **323,** 301–304.

——, 1987: Parameter sensitivity of primitive equation ocean general circulation models. *J. Phys. Oceanogr.,* **17,** 970–985.

Fiadeiro, M. E., and G. Veronis, 1977: On weighted-mean schemes for the finite-difference approximation to the advection–diffusion equation. *Tellus,* **29,** 512–522.

Gordon, A. L., 1986: Interocean exchange of thermocline water. *J. Geophys. Res.,* **91,** 5037–5046.

Hall, M. M., and H. L. Bryden, 1982: Direct estimates and mechanisms of ocean heat transport. *Deep-Sea Res.,* **29,** 339–359.

Killworth, P. D., 1985: A two-level wind and buoyancy driven thermocline model. *J. Phys. Oceanogr.,* **15,** 1414–1432.

Manabe, S., and R. J. Stouffer, 1988: Two stable equilibria of a coupled ocean–atmosphere model. *J. Climate,* **1,** 841–866.

Marotzke, J., 1989: Instabilities and steady states of the thermohaline circulation. *Ocean Circulation Models: Combining Data and Dynamics,* D. L. T. Anderson and J. Willebrand, Eds., Kluwer, 501–511.

——, P. Welander and J. Willebrand, 1988: Instability and multiple equilibria in a meridional-plane model of the thermohaline circulation. *Tellus,* **40A,** 162–172.

Meehl, G. A., W. M. Washington and A. J. Semtner, 1982: Experiments with a global ocean model driven by observed atmospheric forcing. *J. Phys. Oceanogr.,* **12,** 301–312.

Rooth, C., 1982: Hydrology and ocean circulation. *Progress in Oceanography,* Vol. 11, Pergamon, 131–149.

Stocker, T. F., and D. G. Wright, 1991: A zonally averaged ocean model for the thermohaline circulation. Part II: Interocean circulation in the Pacific-Atlantic basin system. *J. Phys. Oceanogr.,* **21,** 1725–1739.

——, D. G. Wright and L. A. Mysak, 1991: A zonally averaged, coupled ocean–atmosphere model for paleoclimate studies. *J. Climate,* in press.

Stommel, H., 1961: Thermohaline convection with two stable regimes of flow. *Tellus,* **13,** 224–230.

Weaver, A. J., and E. S. Sarachik, 1990: On the importance of vertical resolution in certain ocean general circulation models. *J. Phys. Oceanogr.,* **20,** 600–609.

——, and ——, 1991a: The role of mixed boundary conditions in numerical models of the ocean's climate. *J. Phys. Oceanogr.,* (in press).

——, and ——, 1991b: Evidence for decadal variability in an ocean general circulation model: An advective mechanism. *Atmos.–Ocean,* **29,** 197–231.

Welander, P., 1986: Thermohaline effects in the ocean circulation and related simple models. *Large-Scale Transport Processes in Oceans and Atmosphere,* J. Willebrand, and D. L. T. Anderson, Eds., Reidel, 163–200.

Wunsch, C., 1984: An eclectic Atlantic Ocean circulation model. Part I: The meridional flux of heat. *J. Phys. Oceanogr.,* **14,** 1712–1733.